Received: 23 July 2020 | Accepted: 21 April 2021

DOI: 10.1111/1365-2656.13515

RESEARCH ARTICLE

Journal of Animal Ecology | BRITISH ECOLOGICAL SOCIETY

A multi-state occupancy model to non-invasively monitor visible signs of wildlife health with camera traps that accounts for image quality

Maureen H. Murray[1] | Mason Fidino[1] | Elizabeth W. Lehrer[1] | Juniper L. Simonis[2] | Seth B. Magle[1]

[1]Department of Conservation and Science, Lincoln Park Zoo, Chicago, IL, USA

[2]Dapper Stats, Portland, OR, USA

Correspondence
Maureen H. Murray
Email: maureenmurray@lpzoo.org

Funding information
Davee Foundation; Abra Prentice Foundation

Handling Editor: Rachel Norman

Abstract

1. Camera traps are an increasingly popular tool to monitor wildlife distributions. However, traditional analytical approaches to camera trap data are difficult to apply to visible wildlife characteristics in single images, such as infection status. Several parasites produce visible signs of infection that could be sampled via camera traps. Sarcoptic mange *Sarcoptes scabiei* is an ideal disease to study using cameras because it results in visible hair loss and affects a broad host range.
2. Here, we developed a multi-state occupancy model to estimate the occurrence of mange in coyotes *Canis latrans* across an urban gradient. This model incorporates a secondary detection function for apparent by-image infection status to provide detection-corrected estimates of mange occurrence.
3. We analysed a multi-year camera trap dataset in Chicago, Illinois, United States, to test whether the apparent occurrence of sarcoptic mange in coyotes *Canis latrans* increases with urbanization or varies through time. We documented visible signs consistent with current or recovering mange infection and variables we hypothesized would improve mange detection: The proportion of the coyote in frame, image blur and whether the image was in colour.
4. We were more likely to detect coyotes with mange in images that were less blurry, in colour, and if a greater proportion of the coyote was visible. Mangy coyote occupancy was significantly higher in urban developed areas with low housing density and higher canopy cover whereas coyote occupancy, mangy or otherwise, decreased with urbanization.
5. By incorporating image quality into our by-image detection function, we provide a robust method to non-invasively survey visible aspects of wildlife health with camera traps. Apparently mangy coyotes were associated with low-density forested neighbourhoods, which may offer vegetated areas while containing sources of anthropogenic resources. This association may contribute to human–wildlife conflict and reinforces posited relationships between infection risk and habitat use. More generally, our model could provide detection-corrected occupancy

Maureen H. Murray and Mason Fidino contributed equally.

estimates of visible characteristics that vary by image such as body condition or injuries.

KEYWORDS
camera trap, coyote, detectability, occupancy models, sarcoptic mange, urbanization, wildlife disease

1 | INTRODUCTION

Motion-triggered trail cameras (hereafter camera traps) have revolutionized wildlife monitoring and are often used to assess species occupancy or abundance patterns (O'Connell et al., 2010; Steenweg et al., 2017). Yet, the images collected by camera traps likely contain more potentially useful information than simply which species were in an image. For example, Gallo et al. (2019) used camera trap images to quantify prey vigilance rates and associate them to the presence or absence of predators in a given area. Likewise, Hofmeester et al. (2020) used camera trap images to quantify numerous phenological events of plants and animals, such as leaf emergence or the presence of year-born young. Such creative uses of camera trap data demonstrate how a variety of ecological questions can be answered by collecting additional information from camera trap images.

Camera traps may also be used to non-invasively monitor some aspects of wildlife health by collecting additional information in camera trap images. For example, several types of parasites produce visible signs of infection, which provide an opportunity to study the distribution of infected hosts with camera traps. Visible lesions consistent with parasite infection such as mycoplasma conjunctivitis (Hotchkiss et al., 2005) and giraffe skin disease (Muneza et al., 2019) have been documented with cameras to facilitate disease surveillance. Another common wildlife disease with visible signs of infection is sarcoptic mange, caused by the mite *Sarcoptes scabiei*, which can infect over 100 species of mammals (Niedringhaus et al., 2019). Mite infestations induce inflammation, lesions and intense itching as they burrow into the skin. In response to this irritation, the host scratches excessively, causing hair loss and wounds that could serve as routes for secondary infections (Pence & Ueckermann, 2002). Because symptomatic and recovering hosts have visible lesions and patches of hair loss, previous studies have used camera traps to examine the distribution of mange infections in space and time (e.g. Carricondo-Sanchez et al., 2017; Oleaga et al., 2011). Although hair loss consistent with mange cannot be used to reliably distinguish actively diseased from recovering individuals, visible lesions in photographs are consistent with lesions from which mites are recovered (Oleaga et al., 2011). Due to its visible lesions and wide host range, sarcoptic mange thus represents an ideal parasite to study using camera traps.

Aside from being a parasite that could be non-invasively sampled with camera traps, there are many reasons to better understand the spatiotemporal distribution of sarcoptic mange. An increase in mange occurrence with urbanization, for example, would have important implications for human–wildlife conflict because coyotes with mange are more likely to be reported as nuisance animals (Murray, Edwards, et al., 2015), likely in part because they can consume more anthropogenic food (Murray, Cembrowski, et al., 2015; Murray, Edwards, et al., 2015). Sarcoptic mange is also a conservation concern; outbreaks have been implicated in population declines for red foxes *Vulpes vulpes* (Baker et al., 2000) and endangered San Joaquin kit foxes *Vulpes macrotis mutica* (Rudd et al., 2019). Thus, accurately predicting the distribution of mange in space and time is important for understanding population dynamics and infection risk in mammal communities.

Of the studies that have used camera traps to estimate the distribution of mange, a common approach is to analyse the number of images of mangy animals of a given species (e.g. Carricondo-Sanchez et al., 2017; Murray et al., 2016; Saito & Sonoda, 2017). This approach, however, may underestimate mange presence because mange could be missed due to poor photo quality. For example, an image may be too blurry to confidently identify lesions or only part of the individual may be in frame. Furthermore, the apparent prevalence of sarcoptic mange appears to fluctuate over time, with peaks observed in winter (e.g. Almberg et al., 2015; Carridonco-Sanchez et al., 2017) or following multi-year cycles (Iacopelli et al., 2020). These patterns may be driven by host or parasite life history, for example, in winter when energetic costs of thermal stress are higher (Cross et al., 2016). However, these patterns may be confounded by the detectability of mange signs in different contexts, for example, reduced vegetation in temperate climates during winter. The observed data are therefore muddied due to the by-image imperfect detection of mange. When this is compounded with spatial issues of species detectability (i.e. a species may be present in a sampled area but not detected), there are multiple levels of uncertainty that must be teased apart to truly identify spatiotemporal correlates of parasites in camera trap images.

To account for imperfect detection of disease, previous studies have used occupancy models, a flexible analytical approach that estimates the likelihood of wildlife disease presence at a given site, time period or demographic group (Cooch et al., 2012). Such an approach accounts for imperfect detection of visible ectoparasites (Eads et al., 2013) and imperfect diagnostic testing for pathogens (i.e. test sensitivity), though current methods likely limit the spatial extent of sampling because they require the time-intensive capture and restraint of individuals within a sampled site to assess disease presence (Colvin et al., 2015; Eads et al., 2013; Lachish et al., 2012). Camera traps could remove the need for such invasive sampling techniques if visible signs of disease can be identified in images, and have recently been used in combination with occupancy models to

understand the relationship between urbanization and sarcoptic mange in coyotes (Reddell et al., 2021). However, camera trap studies focused on understanding disease presence should also consider how image quality may impact the ability to identify visible signs of disease.

In this study, we developed a multi-state occupancy model to predict the occurrence of sarcoptic mange in coyotes over a gradient of urbanization in Chicago, IL, United States. This model not only accounts for the detectability of coyote across sampling locations but it also accounts for the detectability of mange signs in individual images of coyote. Our approach incorporates apparent by-image infection status within a multi-state occupancy model to account for factors that could impact the detectability of mange infestation such as the clarity of the image and how much of the coyote's body is visible in an image. Based on previous associations between mange and human development, we predicted that the occurrence of coyotes with mange would increase with urban development. We also predicted that the occurrence of mange would increase in periods of thermal stress (i.e. winter), but we were uncertain whether occurrence would follow an annual or multi-year cycle. Lastly, we predicted that our ability to detect mange in an image would increase with image clarity, in colour (daytime) images relative to black and white infrared images taken at night and in images with a greater proportion of the coyote's body in frame. Our approach advances the use of camera traps in wildlife ecology and wildlife disease investigation using non-invasive techniques.

2 | MATERIALS AND METHODS

2.1 | Study area, coyote sampling and spatial covariates

This study was located within the Chicago metropolitan area in northeastern Illinois, United States (hereafter Chicago metro area). The Chicago metro area is located southwest of Lake Michigan and is the third largest metropolitan area in the United States with an estimated 9.9 million residents, 27% of which live in Chicago itself (U.S. Census Bureau, 2018). The Chicago metro area has warm summers (mean = 22.11°C), cold winters (mean = −3.11°C) and intermediate springs (mean = 9.22°C) and autumns (mean = 11.39°C; NOAA, 2019).

To sample the distribution of coyote with and without sarcoptic mange, we set camera traps in urban greenspace (e.g. city parks, cemeteries, natural areas and golf courses) throughout the Chicago metro area (Gallo et al., 2017). We deployed camera traps along three 50-km transects that extended from Chicago's urban centre and travelled northwest, west or southwest along gradients of housing density and impervious cover (Figure 1). We randomly selected a maximum of five sampling locations (hereafter sites) per 5 km section of a transect and sampled 113 sites total. Sites were at least 1 km apart. We deployed cameras for 28 days per sampling season in the winter (January), spring (April), summer (July) and autumn (October). We sampled for 16 consecutive seasons between spring 2010 and winter 2014.

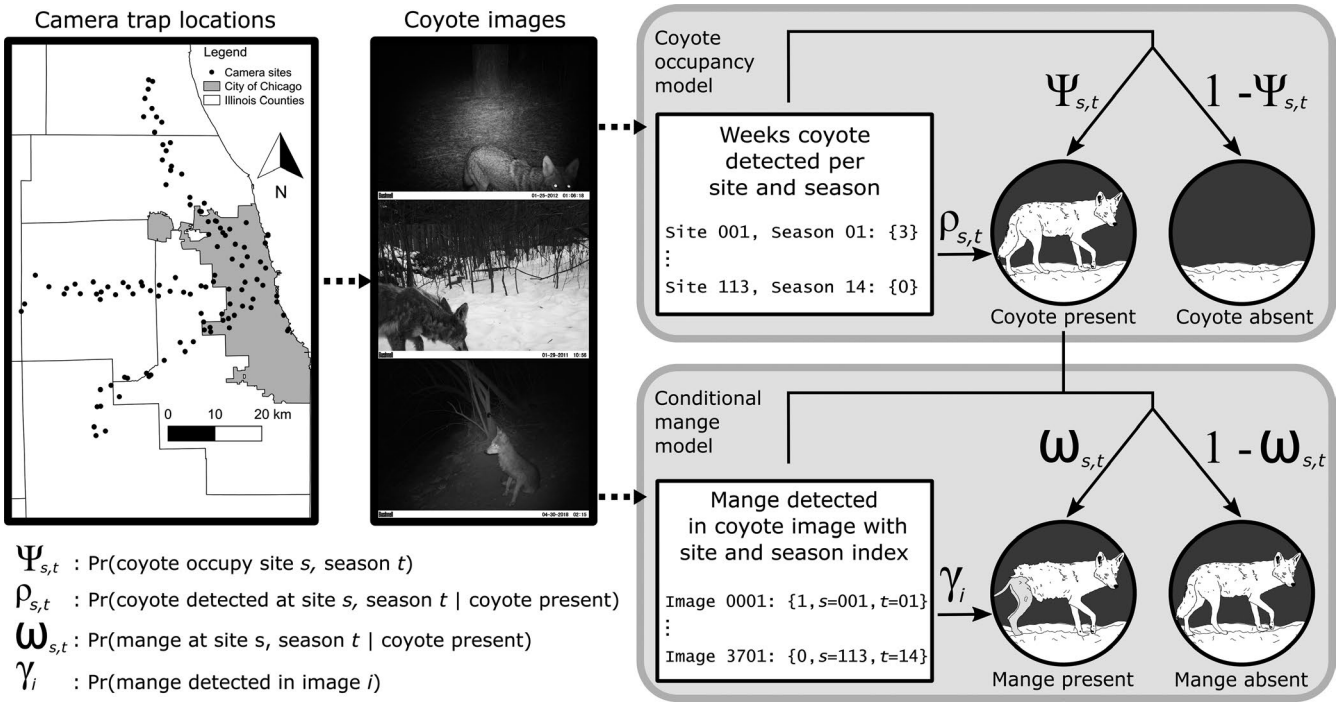

FIGURE 1 Schematic of our multi-state occupancy model to estimate the occurrence of coyotes and mange. We used images of coyotes collected along transects following an urban gradient in the Chicago metro area in a standard single-species multi-season model with a stacked design. Following the coyote occupancy model, our mange model estimates the distribution of coyote with sarcoptic mange conditional on the distribution of coyote, mangy or otherwise, using by-image variation in the presence of mange signs and the quality of the image

At each site, we set one Bushnell motion-triggered infrared TrophyCam roughly 1–1.5 m from the ground on a tree or fence post (see Appendix S1 for models and specifications). We also attached one nylon pouch housing a fatty acid scent lure to another tree about 3–5 m from the camera trap and roughly 0.1 m from the ground (USDA Wildlife Services). Lure was used to potentially increase species detectability, though we have since learned this effect is negligible for coyotes throughout the Chicago metro area (Fidino et al., 2020). We placed sticks between the tree and top of the camera to angle it in a downward trajectory such that the centre of the camera's viewshed was directed at the lure. Sites were revisited once about halfway through each 28-day sampling season to replace memory cards and replace batteries as needed.

To quantify the degree of urbanization around each site, we collected three spatial covariates within a 1,000-m buffer of each camera trap location: housing density (units/km^2), impervious cover (percent) and canopy cover (percent). Housing density data were collected from the Silvis lab data layers (Hammer et al., 2004) whereas impervious cover and canopy cover were collected from the high-resolution (0.6 m^2) data layers available from the Chicago Metropolitan Agency for Planning (CMAP, 2018). We applied a principal component analysis to these data and retained the first two factors which explained 94.30% of the data variability. The variable loadings for the first factor (URB1) were housing density (0.57), impervious cover (0.63) and canopy cover (−0.52). Negative values of URB1 therefore represent sites with high canopy cover (i.e. forest) whereas positive URB1 values are sites with high impervious cover and housing density (i.e. the built environment). The variable loadings for the second factor (URB2) were housing density (0.61), impervious cover (0.10) and canopy cover (0.78). Thus, negative URB2 scores indicate sites with lower levels of canopy cover and housing density (e.g. fields and other open areas) whereas positive URB2 scores indicate sites with more houses and tree cover (i.e. forested neighbourhoods). All spatial covariates were mean-centred and scaled to have a standard deviation of 1. Spatial analyses were carried out in R v 4.0 (R Core Team, 2020).

2.2 | Image processing and image covariates

Images from camera traps were identified to the species level by trained experts. Following this, coyote images were visually assessed a second time by MM to confirm species-level identification of coyote and identify any lesions on the photographed coyote compatible with sarcoptic mange. A coyote in an image was considered to have lesions consistent with sarcoptic mange (hereafter 'mangy') if they had visible areas of hair loss and skin thickening on the tail, haunches, lower back and face, although in severe cases, hair loss may occur on the whole body (Figure 2). We did not consider coyotes as appearing mangy if they had poor body condition without hair loss in the aforementioned areas or if hair loss could be compatible with an injury (e.g. small isolated lesion). A single observer identified images with compatible lesions; any unclear images were checked by at least one other observer (MM or MF). A subset of images (n = 20) classified as containing a mangy coyote was sent for external verification to a wildlife veterinarian familiar with sarcoptic mange (K. Neidringhaus, pers. commun). All but two images were considered compatible with visible signs of active or recovered mange infections. The remaining two images were not clear enough (i.e. too blurry) to confidently verify signs compatible with mange and these images were not classified as containing a mangy coyote in the analysis. Because the detectability function in our model can help correct for false absences but not false presence (see section 'Conditional mange model' below), we erred on the side of caution when classifying mange presence in the remaining coyote images.

Just as camera traps imperfectly sample coyote occurrence, classifying mange within a coyote image is subject to imperfect detection. Therefore, we compiled three variables we hypothesized could influence mange classification. These variables were whether an image was in colour (i.e. taken during the day), what proportion of the coyote's body was visible and the clarity of an image. We also recorded if there were multiple coyotes in frame as this would increase the amount of coyote available in an image to observe for mange, though this was not included as an independent variable because it only occurred in 3.7% of coyote images. To

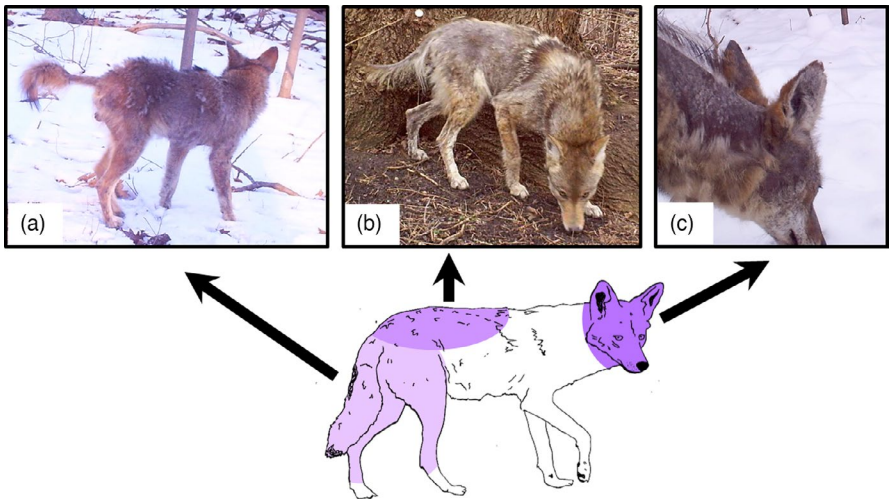

FIGURE 2 We visually assessed remote camera images of coyotes for the presence of hair loss and lesions consistent with sarcoptic mange. Following infestation with the mite *Sarcoptes scabiei*, hair loss and skin thickening typically occur in the shaded regions of the coyote illustration from left to right, beginning on (a) the back of the hind legs and progressing to the haunches and tail, (b) up along the back and (c) then on the ears and face

quantify image clarity, we used Python ver 3.7.1 and the OpenCV package ver 4.3.0 to convolve the greyscale channel of each image with a 3 × 3 Laplacian kernel and then calculated the variance of this response (Pertuz et al., 2013). More positive values of this clarity metric indicate increased image sharpness. Following this, images were classified as 'sharp' if their clarity metric was greater than or equal to the mean clarity (mean = 547.83, min = 46.00, max = 21,171.59). See supplemental material for examples of images that vary in clarity.

2.3 | Statistical analysis

We developed a multi-state occupancy model to jointly estimate coyote occurrence, mangy or otherwise, and the conditional distribution of coyote with mange. Unlike other multi-state models that use a multinomial or categorical distribution to estimate the likelihood of >2 states (e.g. Fidino et al., 2019), we used a set of conditional binomials to accommodate varying levels of imperfect detection that occur across the sampling process. We first explain the coyote occurrence model and then the mange model that is conditional on coyote occurrence at each site. We used a Bayesian framework to jointly estimate these quantities.

2.4 | Coyote occurrence model

This model is a standard single-species multi-season model with a stacked design, and is the first component of our multi-state occupancy model (Figure 1). Let $z_{s,t}$ represents the occupancy status for coyote at site s in 1, …, S and t in 1, …, T seasons. If coyote are present, $z_{s,t} = 1$; otherwise, it is 0. We model the spatiotemporal occurrence of coyote as the following Bernoulli process:

$$z_{s,t} \mid \psi_{s,t} \sim \text{Bernoulli}(\psi_{s,t}),$$

where $\psi_{s,t}$ is the probability that coyote, mangy or otherwise, occupies site s on season t. We used the logit-link to allow $\psi_{s,t}$ to be a logit-linear function of our two urbanization covariates, their interaction, a temporal random effect and a temporal auto-logistic term to account for temporal dependence in occupancy from one season to the next (Royle & Dorazio, 2008). Thus, for the first season of sampling, the log-linear predictor of occupancy is

$$\text{logit}(\psi_{s,t=1}) = a_0 + a_1 Urb1_s + a_2 Urb2_s + a_3 Urb1_s Urb2_s + u_{t,1},$$

where $u_{t,1} \sim \text{Normal}(0, \sigma_\Psi)$. For the following seasons, we account for temporal autocorrelation with the auto-logistic term, θ_1:

$$\text{logit}(\psi_{s,t>1}) = a_0 + a_1 Urb1_s + a_2 Urb2_s + a_3 Urb1_s Urb2_s + u_{t,1} + \theta_1 z_{t-1}.$$

We used the simpler auto-logistic formulation in favour of a dynamic occupancy model that estimates colonization and extinction probabilities among seasons to accommodate the relative sparsity of mange detections in our dataset. However, this model can be replaced with a dynamic occupancy model if sufficient data are available to accommodate the additional model complexity.

Coyote occurrence is imperfectly sampled. Let $y_{s,t}$ represents the number of weeks a coyote was observed at site s and season t, which can be summarized from the camera trap data. The probability of detecting coyote given their presence (i.e. $z_{s,t} = 1$), can be modelled as a binomial process.

$$y_{s,t} \mid z_{s,t}, \rho_{s,t} \sim \text{Binomial}(n_{s,t}, \rho_{s,t} z_{s,t}).$$

Here, $\rho_{s,t}$ represents the conditional weekly probability of detecting coyote, mangy or otherwise, at site s and season t, while $n_{s,t}$ is the number of weeks sampled. We used the logit-link to allow $\rho_{s,t}$ to vary via the average monthly temperature of a season as well as a temporal random effect.

$$\text{logit}(\rho_{s,t}) = b_0 + b_1 \text{temp}_t + u_{t,2},$$

where $u_{t,2} \sim \text{Normal}(0, \sigma_\rho)$. Average monthly temperature was included because visible obstruction from leaves as well as coyote activity patterns, and therefore their detectability, may shift with temperature (Gese et al., 1988, 1996). Temperature data were collected from NOAA (2019).

2.5 | Conditional mange model

The mange model estimates the distribution of coyote with sarcoptic mange conditional on the distribution of coyote, mangy or otherwise. As such, we are estimating the occurrence of apparent mange (i.e. the presence of apparent mange based on detections) rather than the prevalence (i.e. the proportion of the study population that is visibly infected). This is an important distinction because infection prevalence is a common metric to assess the distribution or risk of infection in wildlife populations. However, infection prevalence cannot be estimated when sampling unidentifiable individual animals, as we are with unmarked coyotes, because individuals might be repeatedly sampled. Let $\omega_{s,t}$ represents the probability a coyote at site s and season t has sarcoptic mange and $x_{s,t}$ represents mangy coyote presence ($x_{s,t} = 1$) or absence ($x_{s,t} = 0$). We link this model to the coyote occurrence model by making $\omega_{s,t}$ conditional on the presence of coyote ($z_{s,t} = 1$), mangy or otherwise:

$$x_{s,t} \mid \omega_{s,t}, z_{s,t} \sim \text{Bernoulli}(\omega_{s,t} z_{s,t}).$$

If coyote are present at site s and season t, then the probability at least one has mange is $\omega_{s,t}$. If coyote are absent, then the probability of mangy coyote is zero (Figure 1). As with the coyote occurrence model, we allow $\omega_{s,t}$ to be a logit-linear function of our two urbanization covariates, their interaction, a temporal random effect and a temporal

auto-logistic term to account for repeat sampling at sites. For the first season, the logit-linear predictor is

$$\text{logit}(\omega_{s,t=1}) = c_0 + c_1 Urb1_s + c_2 Urb2_s + c_3 Urb1_s Urb2_s + u_{t,3},$$

where $u_{t,3} \sim \text{Normal}(0, \sigma_\omega)$ while for seasons after the first season, it is

$$\text{logit}(\omega_{s,t>1}) = c_0 + c_1 Urb1_s + c_2 Urb2_s + c_3 Urb1_s Urb2_s + u_{t,3} + \theta_2 z_{t-1}.$$

Unlike the coyote occurrence model which treats sampling weeks as secondary observations, we have individual coyote images across sites and seasons where mange on a coyote may be missed due to photo quality. The number of coyote images per site and season also varies. To account for this by-image variability in sampling and photo quality, we model them individually. Thus, for *i* in 1, ..., *I* coyote photos across the entire study, let q_i represent if mange was detected (q_i = 1) or not detected (q_i = 0) in photo *i*. Additionally, let ***site*** and ***season*** represent vectors of length *I* that denote what site (i.e. *s*) and season (i.e. *t*) each photo was taken. For example, if photo $i = 3$ was taken at site $s = 15$ and season $t = 1$, then $site_3 = 15$ and $season_3 = 1$. With this specification, the ***site*** and ***season*** vectors can be used to connect the coyote mange latent state that varies by site and season to an observation model that varies by image via the nested indexing of $x_{s,t}$:

$$q_i \,|\, x_{s,t}, z_{s,t} \sim \text{Bernoulli}\left(\gamma_i x_{[\text{site}_i, \text{season}_i]}\right).$$

Here, let γ_i represents the conditional probability mange is detected in a coyote image given a mangy coyote is present. γ_i is then made a logit-linear function of whether an image was taken during the day (DAY_i), the proportion of the coyote visible in an image (VIS_i) and whether the image was not blurry (CLR_i):

$$\text{logit}(\gamma_i) = d_0 + d_1 \text{DAY}_i + d_2 \text{VIS}_i + d_3 \text{CLR}_i.$$

2.6 | Priors and model run specification

We gave all logit-scale parameters uninformative logistic(0,1) priors and the three random effect terms (***u***) their own respective Normal(0,σ) priors where σ ~Inv-Gamma(1,1). We fit this model in JAGS v 4.3.0 (Plummer, 2003) via the runjags package (Denwood, 2016) in R ver. 4.0.0 (R Core Team, 2020). Six chains were used and following a 1,000 step adaptation and 25,000 step burn-in, chains were sampled 33,334 times each. Chains were thinned by 2 for a total of 100,002 posterior samples. We assessed model convergence by visually inspecting traceplots for proper mixing and ensured Gelman–Rubin diagnostics for each parameter were <1.10 (Gelman et al., 2013).

We provided evidence for an effect in two ways. First, we determined how much of each parameter's posterior was greater or less than zero, depending on the direction of the effect. This approach is a useful feature of Bayesian analyses as it is possible to make probability statements derived from posterior probability distributions (Hobbs & Hooten, 2015; Kéry, 2010). Second, we calculated 95% Bayesian credible intervals (BCI) and evaluated whether they overlapped zero. For model evaluation, we calculated binned residuals for each linear predictor of our model following Wright et al. (2019). Binned residuals did not show any apparent positive or negative bias, which indicates the model did a sufficient job fitting the data (see Appendix S2 for model diagnostics). As an example, we also simulated a single season's worth of data with parameters of similar magnitude to what we retrieved from the model fit to our actual data and compared parameter estimates to the true values used to simulate the data. The true parameter values were within the 95% credible interval of each parameter estimate. See Appendix S3 for simulation code simulation results.

2.7 | Landscape predictions

With this model, $\omega_{s,t}$ is the probability of mange given the presence of coyote and $\psi_{s,t}$ is the probability of coyote occurrence, mangy or otherwise. As such, the probability of the three possible states in which a site could be—no coyote, coyote without mange, coyote with mange—is $(1 - \psi_{s,t})$, $(1 - \omega_{s,t})\,\psi_{s,t}$ and $\omega_{s,t}\,\psi_{s,t}$, respectively, which sum to one. With the median estimates from our model, we extrapolated the occupancy probability of coyote, mangy or otherwise ($\psi_{s,t}$), and the probability of mangy coyote ($\omega_{s,t}\,\psi_{s,t}$) across our study region. To do so, we created a grid of points (n = 28,329) spaced 400 m apart across the study area. We extracted the same spatial predictor variables (canopy cover, impervious surface and housing density), scaled them to the spatial data collected at our sites and then calculated the urbanization metrics (URB1 and URB2) and their interaction using the variable loadings from our PCA. With the inclusion of the auto-logistic term, expected occupancy estimates are more complicated to calculate than with a standard single-season occupancy model. However, this auto-logistic representation is an alternative parameterization of a dynamic occupancy model (Royle & Dorazio, 2008). Thus, given mean-centred covariates, the average occupancy of coyote, mangy or otherwise, can be derived as

$$\overline{\psi} = \text{expit}(a_0)/(\text{expit}(a_0) + (1 - \text{expit}(a_0 + \theta_1))),$$

where expit is the inverse logit function. Similarly, site-specific predictions can be derived by including the associated slope terms and covariates into $\text{expit}(a_0)$ and $\text{expit}(a_0 + \theta_1)$.

3 | RESULTS

Of a possible 7,232 sampling weeks (113 sites × 16 seasons × 4 weeks), we collected 5,007 weeks of data, which resulted in 3,701 coyote images. We collected an average of 231.31 coyote images, mangy or otherwise, per season (min = 39, max = 518) and 6.90 coyote images per site and season (min = 1, max = 60). We detected mange in 199 of the 3,701 coyote images (5.38%). We collected an average of 12.4 mangy coyote images per season (min = 2, max = 33)

and 0.37 mangy coyote images per site and season (min = 0, max = 10). Average coyote naive occupancy, mangy or otherwise, was 0.45 (min = 0.31 max = 0.56). Across all seasons, coyote, mangy or otherwise, was photographed at 78% of the 113 sites. Average mangy coyote naive occupancy was 0.15 (min = 0.05, max = 0.29). Across all seasons, mangy coyote was photographed at 39% of the 113 sites.

3.1 | Coyote occupancy, mangy or otherwise

As a reminder, the built environment covariate (URB1) represents a gradient of high canopy cover to high impervious cover and housing density while the forested neighbourhoods covariate (URB2) represents a gradient of increasing levels of canopy cover and housing density. Average coyote occupancy across seasons was 0.53 (95% BCI = 0.40, 0.67). Coyote occupancy decreased with increasing URB1 (a_1 = −0.60, 95% BCI = −0.73, −0.47) and URB2 (a_2 = −0.20, 95% BCI = −0.40, 0.00), but increased with the interaction of URB1 and URB2 (a_3 = 0.16, 95% BCI = 0.08, 0.24). Therefore, coyote occupancy was at its greatest when URB1 and URB 2 were both negative, which represents sites with high levels of canopy cover and low levels of impervious cover and housing density (Figure 3a). For example, our five sampled sites with the most negative URB1 and URB2 values were 4.83 (95% CI = 2.11, 9.06) times more likely to be occupied by coyote, mangy or otherwise, than our five sampled sites with the most positive URB1 and URB2 values. On average, sites with coyote, mangy or otherwise, in the current time-step were 3.13 (95% BCI = 2.40, 4.29) times more likely to have coyote in the next time-step (θ_1 = 2.38, 95% BCI = 1.91, 2.90). Among season variation in coyote occupancy, σ_Ψ, was 0.64 (95% BCI = 0.43, 1.01), assuming normal variation in occupancy on the logit scale.

Average weekly detection probability of coyote was 0.45 (95% BCI = 0.38, 0.51). Given this estimate, there was a 0.90 (95% BCI = 0.85, 0.94) probability of detecting coyote at a site if they were present with 4 weeks of sampling. There was some evidence that coyote detectability decreased with increasing temperature (b_2 = −0.19, 95% BCI = −0.47, 0.09), but we are only 91.71% certain this effect was less than zero. Among season variation in coyote detectability, σ_ρ, was 0.49 (95% BCI = 0.35, 0.74).

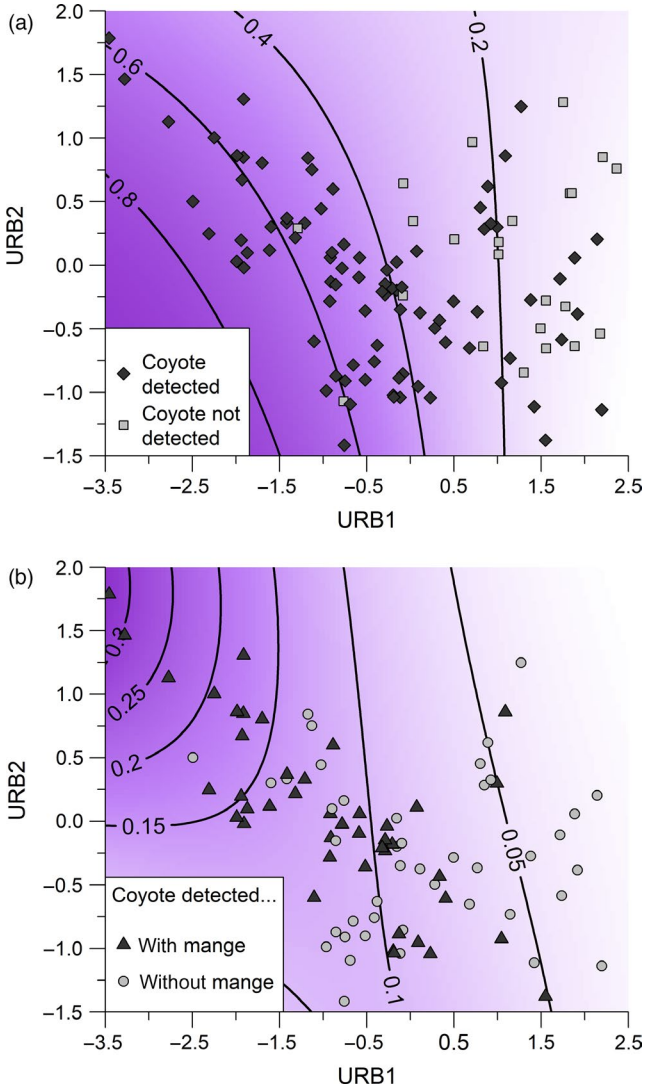

FIGURE 3 Relationships between urbanization and the occurrence of (a) coyotes, mangy or otherwise, and (b) mangy coyotes. URB1 and URB2 are two axes of a PCA used to quantify urbanization. Positive values of URB1 represent built areas while positive values of URB2 represent low-density forested neighbourhoods. Triangles represent camera sites where (a) coyotes or (b) mangy coyotes were detected in at least one season. Shaded regions and contour lines indicate habitat types where (a) coyotes or (b) mangy coyotes are more likely to occur

3.2 | Coyote with mange occupancy

Across seasons, sites with coyote had a 0.35 (95% BCI = 0.21, 0.55) probability of containing a coyote with mange (i.e. $E[\omega_{s,t}]$). The average occupancy of mangy coyote, $E[\omega_{s,t}\,\psi_{s,t}]$, was 0.19 (95% BCI = 0.11, 0.31). Given the posterior estimates, we are only 74.52% certain that the effect of URB1 on mangy coyote was nonzero and that the sign was positive (c_1 = 0.11, 95% BCI = −0.22, 0.44). There was also little evidence URB2 was associated with the spatial distribution of mangy coyote (c_2 = 0.07, 95% BCI = −0.47, 0.55).

Mangy coyote occupancy did, however, decrease with the interaction of URB1 and URB2 (c_3 = −0.31, 95% BCI = −0.68 to −0.06). Plotting out this relationship illustrates mangy coyote occupancy was at its greatest when URB1 was negative (i.e. high canopy cover), but URB2 was positive (i.e. canopy cover with intermixed housing; Figure 3b). For example, our five sampled sites with the most negative URB1 and most positive URB2 values were about 3.12 (95% BCI = 0.85, 17.33) times more likely to have a coyote with mange than our five sampled sites with the most positive URB1 and URB2 values. On average, sites with mangy coyote in the current time-step were 2.57 (95% BCI = 1.38, 4.56) times more likely to have mangy coyote in the next time-step (θ_2 = 1.58, 95% BCI = 0.50, 2.66). Among season variation in mangy coyote occupancy, σ_ω, was 0.64

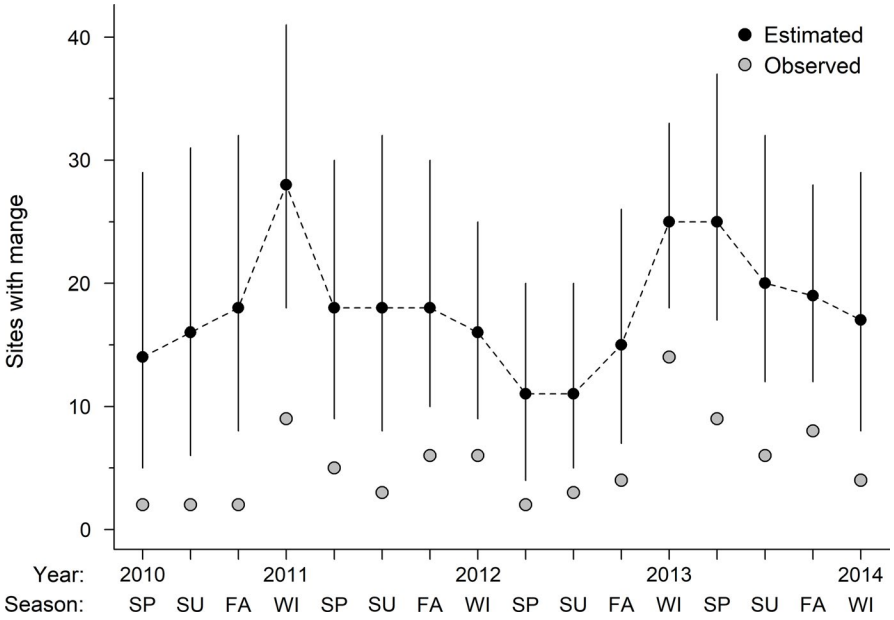

FIGURE 4 The number of camera sites at which we detected mangy coyotes in photographs (observed, grey circles) versus the number of sites estimated by our multi-state occupancy model (black circles) in the 16 study seasons. Cameras were active for one month each calendar quarter (SP = spring, April; SU = summer, July; FA = fall, October; WI = winter, January). Error bars on estimated values show 95% Bayesian confidence intervals

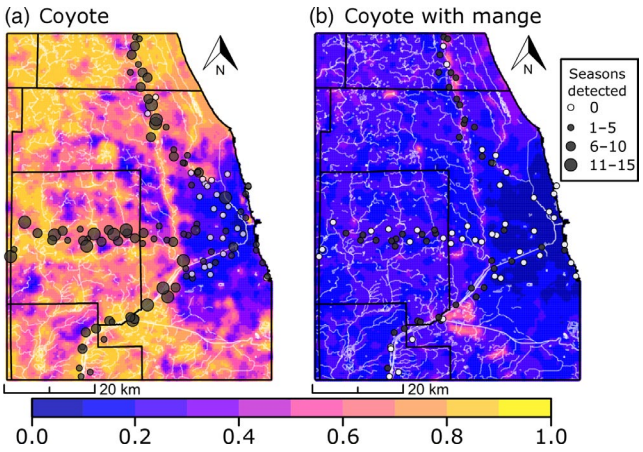

FIGURE 5 Map of the Chicago metro area showing the predicted probability of (a) coyote, mangy or otherwise and (b) mangy coyote occurrence, from 0 (dark blue) to 1 (yellow). White lines represent rivers and streams while black lines represent county boundaries

(95% BCI =0.41, 1.07). We did not observe any consistent seasonal differences in mange occurrence across the 16 sampling seasons (Figure 4).

Of the 3,071 coyote images we collected, 9.92% were clear daytime images, 4.5% were blurry daytime images, 29.72% were clear night-time images and 55.85% were blurry night-time images. The probability of detecting mange in coyote images increased if the image was taken during the day (d_1 = 1.17, 95% BCI = 0.76, 1.59), if more of the coyote was visible (d_2 = 1.06, 95% BCI = 0.83, 1.32), and if the image was not blurry (d_3 = 0.45, 95% BCI = 0.06, 0.84). Given an average amount of coyote visible in an image (mean VIS_i = 0.34, min = 0.01, max = 0.55), there was a 0.08 (95% BCI = 0.06, 0.10) probability of detecting mange given mange presence in a blurry night-time coyote image, which were the most commonly collected coyote image. The probability of detecting mange given mange presence was highest for clear (i.e. less blurry than the average image) daytime images (0.29, 95% BCI = 0.23, 0.37), followed by blurry daytime images (0.21, 95% BCI = 0.14, 0.30), then clear night-time images (0.11, 95% BCI =0.08, 0.16). Blurry night-time images had the lowest probability of mange detection.

3.2.1 | Landscape predictions

Using median estimates from our model, we predicted the probability of coyote occupancy, mangy or otherwise (Figure 5a), and the probability of mangy coyotes throughout the Chicago metro area (Figure 5b). Our model predicted cool spots (<0.20 probability) for both groups of coyotes in the downtown core and predicted several isolated hotspots (>0.40 probability) for mangy coyotes. The hotspots for mangy coyote were primarily along rivers or located in parts of the metro area that had low housing density and high tree cover (e.g. North of Chicago).

4 | DISCUSSION

In this study, we analysed camera trap data with a multi-state occupancy model to estimate the occurrence of sarcoptic mange in coyotes over urbanization gradients. This approach enabled us to quantify the probability of mangy coyote occupancy while accounting for the effects of image quality on the detectability of mange signs. Overall, we found that mangy coyotes were more likely to occur in areas with low-density urban development relative to visibly healthy coyotes, but image quality severely influenced the probability of detecting mange given its presence. For example, over half of the coyote images we collected were blurry night-time images, which only had about a 0.07 probability of mange detection if it was

present. By accounting for by-site and by-image uncertainty, our model provides detection-corrected estimates of a species distribution and how health characteristics of that species may change within that distribution (e.g. the likelihood of sarcoptic mange). Thus, our model offers several advancements for non-invasively measuring the occurrence of visible characteristics of wildlife over large spatial and temporal scales.

Heterogeneity in image quality greatly influenced the detectability of mange signs. For instance, a higher proportion of a coyote's body in frame increased our likelihood of detecting visible mange lesions. This is unsurprising, because images containing more of the body's surface area offer greater opportunities to see lesions only present in one area. To maximize body visibility, cameras could be positioned in pairs to capture both sides of the animal or set to take multiple images when triggered. Increased body visibility also permits better estimates of the severity of infection, which can be indicative of mite load. For example, mite load increased with the percentage of mange damaged skin in Iberian wild goats *Capra pyrenaica* (Pérez et al., 2011) but was negatively correlated with the percentage of damaged skin in wolves *Canis lupus* (Oleaga et al., 2011). In this way, visible estimates may be important in determining parasite dynamics in free-living wildlife populations. We were also more likely to detect mange in colour photos (i.e. during the day), and so the activity patterns of focal species could affect camera monitoring. Although less important than the aforementioned factors, we were more likely to detect mange signs in clearer (i.e. less blurry) images. Image clarity might have had a stronger effect if we were able to discern the blurriness of the coyote separate from its surroundings. For instance, in some images, the coyote was in focus while vegetation nearer the camera was blurry. Our quantification of image blurriness appears to be novel for wildlife camera trap research and could be increasingly important as machine-learning tools to automatically identify wildlife species become more popular (e.g. Tabak et al., 2019). We recommend that future studies place cameras at locations where animals move more slowly or pause (e.g. at a scent post) to reduce blurred images and improve detection rates. Understanding these relationships between image quality and detectability will thus help improve the design of camera trap studies and model estimates.

Using our modelling approach, we found that mangy coyote occupancy was higher in developed areas with low housing density and higher canopy cover (i.e. negative URB1 but positive URB2). These low-density neighbourhoods may offer vegetated areas and contain anthropogenic resources. Habitat at the interface of residential and natural areas is often selected by coyotes presumably because they offer high prey availability, visual cover and anthropogenic food (Murray & St. Clair, 2017). These areas may be especially attractive to mangy coyotes as these individuals are more likely to scavenge rather than hunt (Todd et al., 1981) and consume anthropogenic foods (Murray, Cembrowski, et al., 2015; Murray, Edwards, et al., 2015). Our results reinforce previously documented associations between mange and urban areas in coyotes (Reddell et al., 2021), peri-urban areas in foxes (Carricondo-Sanchez et al., 2017) and partially forested suburban landscapes in raccoon dogs (Saito & Sonoda, 2017). These similar results among species and locations suggest that not accounting for by-image mange detectability in previous studies likely underestimated mange occurrence (i.e. naïve occurrence vs. true occurrence) but did not introduce systematic biases in mange detection in different habitats.

In contrast with mangy coyotes, site occupancy by coyotes, mangy or otherwise, decreased with urbanization, supporting previous work on urban coyote habitat use in the region. Long-term monitoring of coyote movement in the Chicago metro area using telemetry shows that although coyotes can make use of the urban matrix (Gehrt et al., 2009), most select for natural areas for home range placement and especially within home ranges (Gehrt & Riley, 2010; Gese et al., 2012). Is it encouraging that our results align closely with those of more fine-scale but more costly and invasive sampling methods. However, there is high variation in coyote occupancy among cities (Fidino et al., 2021); for example, coyotes in Denver generally had a high degree of urban development within home ranges (Poessel et al., 2016). Understanding urban coyote distributions within cities will help predict potential conflicts and potentially parasite risk (Werner & Nunn, 2020).

Although we found evidence of spatial variation in the occurrence of mange in urban coyotes, seasonal patterns appeared to be relatively random. We detected coyotes with mange at more sites in winter 2011 and winter 2013 (Figure 4), providing some support to our prediction that mange could be more prevalent or severe because of environmental stressors. However, this trend was not consistent during the middle year of our study. This pattern may indicate that sarcoptic mange in this system peaks on a multi-year cycle, as it does in other species (e.g. Iacopelli et al., 2020). As teasing apart multi-year periodic cycles requires longer time series to accurately estimate trends (Fidino & Magle, 2017), it is likely that more data will be necessary to determine if seasonal changes in coyote mange occurrence follow a specific multi-year pattern. Nevertheless, our results illustrate how multi-year projects are important to understand mange dynamics in wildlife.

We used our model to predict the probability of coyote occurrence, mangy or otherwise, and the probability of mangy coyote occurrence across the Chicago metro area. In both cases, we detected cool spots in highly urban areas and hot spots near riparian areas along the Des Plaines river in the North and Southwest of Chicago (Figure 5). Although coyotes typically exhibit high mobility in urban landscapes (e.g. Poessel et al., 2016), major roads can still present a barrier to many species (Holderegger & Di Giulio, 2010) and these riparian areas may help to facilitate movement for coyotes. Areas with high connectivity such as wildlife corridors have been hypothesized to promote the transmission of pathogens between wildlife populations by increasing contact between dispersing individuals (Remais et al., 2010). Understanding the association between landscape connectivity and pathogen transmission for wildlife in highly fragmented urban systems would be important for mitigating effects and is a fruitful avenue for future research.

Identifying hot spots of mange occurrence can help inform managers of specific habitats with higher risk of disease and potential for

human–wildlife conflict. For instance, managers could prioritize sites with a higher likelihood of mange occurrence to manage coyote attractants that might promote parasite spread. Importantly, our conditional mange model estimates the likelihood of mange occurrence at a particular site, rather than a higher prevalence of mange (i.e. the proportion of coyotes that are symptomatic). This focus on site occurrence is less information-rich compared to estimating prevalence, but it facilitates non-invasive monitoring while avoiding assumptions about identifying individual animals in images. Furthermore, estimates of site occurrence are less sensitive to disease surveillance methodology such as sampling an adequate proportion of the population or whether individual hosts can be considered independent samples. To get the best of both worlds, managers could select priority sites with our modelling approach for more intensive disease surveillance in high-risk areas.

In this study, we developed a multi-state occupancy model to address multiple levels of sampling uncertainty to quantify the occurrence of mange in coyotes along an urbanization gradient. Such an approach minimizes issues with measuring disease prevalence using non-invasive methods in unmarked populations. By incorporating image quality in our by-image detection function, we provided more robust estimates of mange occurrence across the urban landscape. Our multi-state occupancy model can also help estimate the occurrence of many other measures of visible wildlife phenomena using camera traps. Remote cameras can be used to document several visible aspects of wildlife health including body condition (e.g. Prosser et al., 2016) and injuries. This approach could also be used to better quantify the occurrence of behavioural states such as vigilance or foraging (Gallo et al., 2019) or the occurrence of different life stages. More generally, incorporating image quality when estimating species occurrence will help account for missed detections based on very blurry images or differences in lighting (e.g. when species identification is based on colour). Expanding the use of camera trapping for novel ecological questions advances non-invasive wildlife research and facilitates studies over larger spatial and temporal scales.

ACKNOWLEDGEMENTS

We thank Dr Kevin Niedringhaus for validating a subset of the photographs containing mangy coyotes. We would also like to thank J. Rios, M. Mulligan and the many interns and volunteers that helped with fieldwork and processing photos. We would also like to thank W. Simonis for their encouragement while M.F. and J.L.S. developed the modelling framework. We are grateful to the many landowners who allowed us access to their property, including the forest preserve districts of Cook, DuPage, Lake and Will counties, the Illinois Department of Natural Resources' Nature Preserve Commission, the Chicago Park District and the Archdiocese of Chicago. This work was supported by the 476 Abra Prentice Foundation and the Davee Foundation. The authors have no conflict of interest to declare.

AUTHORS' CONTRIBUTIONS

M.H.M. developed the idea for this manuscript; M.F. and J.L.S. developed the modelling framework; M.F. analysed the data; M.H.M. and M.F. wrote the first draft of the manuscript; M.H.M., M.F., E.W.L. and S.B.M. collected and summarized data. All authors contributed to additional revisions of the manuscript.

DATA AVAILABILITY STATEMENT

All code and data are available on github at https://github.com/mfidino/coyote-mange and are archived on Zenodo https://doi.org/10.5281/zenodo.4721850 and Dryad Digital Repository https://doi.org/10.5061/dryad.x3ffbg7js (Murray et al., 2021).

ORCID

Maureen H. Murray https://orcid.org/0000-0002-2591-0794
Mason Fidino https://orcid.org/0000-0002-8583-0307
Juniper L. Simonis https://orcid.org/0000-0001-9798-0460
Seth B. Magle https://orcid.org/0000-0003-0275-3885

REFERENCES

Almberg, E. S., Cross, P. C., Dobson, A. P., Smith, D. W., Metz, M. C., Stahler, D. R., & Hudson, P. J. (2015). Social living mitigates the costs of a chronic illness in a cooperative carnivore. *Ecology Letters*, *18*, 660–667. https://doi.org/10.1111/ele.12444

Baker, P. J., Funk, S. M., Harris, S., & White, P. C. L. (2000). Flexible spatial organization of urban foxes, *Vulpes vulpes*, before and during an outbreak of sarcoptic mange. *Animal Behaviour*, *59*, 127–146. https://doi.org/10.1006/anbe.1999.1285

Carricondo-Sanchez, D., Odden, M., Linnell, J. D. C., & Odden, J. (2017). The range of the mange: Spatiotemporal patterns of sarcoptic mange in red foxes (*Vulpes vulpes*) as revealed by camera trapping. *PLoS ONE*, *12*(4), 1–16. https://doi.org/10.1371/journal.pone.0176200

Chicago Metropolitan Agency for Planning Data Hub. (2018). *High-resolution Land Cover, NE Illinois and NW Indiana*. Retrieved from https://datahub.cmap.illinois.gov/dataset/high-resolution-land-cover-ne-illinois-and-nw-indiana-2010

Colvin, M. E., Peterson, J. T., Kent, M. L., & Schreck, C. B. (2015). Occupancy modeling for improved accuracy and understanding of pathogen prevalence and dynamics. *PLoS ONE*, *10*, e0116605. https://doi.org/10.1371/journal.pone.0116605

Cooch, E. G., Conn, P. B., Ellner, S. P., Dobson, A. P., & Pollock, K. H. (2012). Disease dynamics in wild populations: Modeling and estimation: A review. *Journal of Ornithology*, *152*, S485–S509. https://doi.org/10.1007/s10336-010-0636-3

Cross, P. C., Almberg, E. S., Haase, C. G., Hudson, P. J., Maloney, S. K., Metz, M. C., Munn, A. J., Nugent, P., Putzeys, O., Stahler, D. R., Stewart, A. C., & Smith, D. W. (2016). Energetic costs of mange in wolves estimated from infrared thermography. *Ecology*, *97*(8), 1938–1948. https://doi.org/10.1890/15-1346.1

Denwood, M. J. (2016). runjags: An R package providing interface utilities, model templates, parallel computing methods and additional distributions for MCMC models in JAGS. *Journal of Statistical Software*, *71*(9), 1–25.

Eads, D. A., Biggins, D. E., Doherty, P. F., Gage, K. L., Huyvaert, K. P., Long, D. H., & Antolin, M. F. (2013). Using occupancy models to investigate the prevalence of ectoparasitic vectors on hosts: An example with fleas on prairie dogs. *International Journal for Parasitology: Parasites and Wildlife*, *2*, 246–256. https://doi.org/10.1016/j.ijppaw.2013.09.002

Fidino, M., Barnas, G. R., Lehrer, E. W., Murray, M. H., & Magle, S. B. (2020). The effect of lure on detecting mammals with camera traps. *Wildlife Society Bulletin*, *44*(30), 543–552.

Fidino, M., Gallo, T., Lehrer, E. W., Murray, M. H., Kay, C., Sander, H. A., MacDougall, B., Salsbury, C. M., Ryan, T. J., Angstmann, J. L., Belaire,

J. A., Dugelby, B., Schell, C., Stankowich, T., Amaya, M., Drake, D., Hursh, S. H., Ahlers, A. A., Williamson, J., … Magle, S. B. (2021). Landscape-scale differences among cities alter common species' responses to urbanization. *Ecological Applications*, *31*(2), e02253.

Fidino, M., & Magle, S. B. (2017). Using Fourier series to estimate periodic patterns in dynamic occupancy models. *Ecosphere*, *8*(9), e01944. https://doi.org/10.1002/ecs2.1944

Fidino, M., Simonis, J. L., & Magle, S. B. (2019). A multistate dynamic occupancy model to estimate local colonization–extinction rates and patterns of co-occurrence between two or more interacting species. *Methods in Ecology and Evolution*, *10*(2), 233–244. https://doi.org/10.1111/2041-210X.13117

Gallo, T., Fidino, M., Lehrer, E. W., & Magle, S. B. (2017). Mammal diversity and metacommunity dynamics in urban green spaces: Implications for urban wildlife conservation. *Ecological Applications*, 1–12. https://doi.org/10.1002/eap.1611

Gallo, T., Fidino, M., Lehrer, E. W., & Magle, S. (2019). Urbanization alters predator-avoidance behaviours. *Journal of Animal Ecology*, *88*(5), 793–803. https://doi.org/10.1111/1365-2656.12967

Gehrt, S. D., Anchor, C., & White, L. A. (2009). Home range and landscape use of coyotes in a metropolitan landscape: Conflict or coexistence? *Journal of Mammalogy*, *90*(5), 1045–1057. https://doi.org/10.1644/08-MAMM-A-277.1

Gehrt, S. D., & Riley, S. P. D. (2010). Coyotes (*Canis latrans*). In S. Gehrt, S. Riley, & B. Cypher (Eds.), *Urban carnivores: Ecology, conflict, and conservation* (pp. 79–95). The Johns Hopkins University Press.

Gelman, A., Carlin, J. B., Stern, H. S., Dunson, D. B., Vehtari, A., & Rubin, D. B. (2013). *Bayesian data analysis*. CRC Press.

Gese, E. M., Morey, P. S., & Gehrt, S. D. (2012). Influence of the urban matrix on space use of coyotes in the Chicago metropolitan area. *Journal of Ethology*, *30*(3), 413–425. https://doi.org/10.1007/s10164-012-0339-8

Gese, E. M., Rongstad, O. J., & Mytton, W. R. (1988). Home range and habitat use of coyotes in southeastern Colorado. *The Journal of Wildlife Management*, *52*(4), 640–646. https://doi.org/10.2307/3800923

Gese, E. M., Ruff, R. L., & Crabtree, R. L. (1996). Social and nutritional factors influencing the dispersal of resident coyotes. *Animal Behaviour*, *52*, 1025–1043. https://doi.org/10.1006/anbe.1996.0250

Hammer, R. B., Stewart, S. I., Winkler, R. L., Radeloff, V. C., & Voss, P. R. (2004). Characterizing dynamics spatial and temporal residential density patterns from 1940–1990 across the North Central United States. *Landscape and Urban Planning*, *69*, 183–199.

Hobbs, N. T., & Hooten, M. B. (2015). *Bayesian models: A statistical primer for ecologists*. Princeton University Press.

Hofmeester, T. R., Young, S., Juthberg, S., Singh, N. J., Widemo, F., Andrén, H., Linnell, J. D., & Cromsigt, J. P. (2020). Using by-catch data from wildlife surveys to quantify climatic parameters and timing of phenology for plants and animals using camera traps. *Remote Sensing in Ecology and Conservation*, *6*(2), 29–140. https://doi.org/10.1002/rse2.136

Holderegger, R., & Di Giulio, M. (2010). The genetic effects of roads: A review of empirical evidence. *Basic and Applied Ecology*, *11*, 522–531. https://doi.org/10.1016/j.baae.2010.06.006

Hotchkiss, E. R., Davis, A., Cherry, J. J., & Alitzer, S. (2005). Mycoplasmal conjunctivitis and the behavior of wild house finches (*Carpodacus mexicanus*) at bird feeders. *Bird Behavior*, *17*, 1–8.

Iacopelli, F., Fanelli, A., Tizzani, P., Berriatua, E., Prieto, P., Martínez-Carrasco, C., León, L., Rossi, L., & Candela, M. G. (2020). Spatio-temporal patterns of sarcoptic mange in red deer and Iberian ibex in a multi-host natural park. *Research in Veterinary Science*, *128*, 224–229. https://doi.org/10.1016/j.rvsc.2019.11.014

Kéry, M. (2010). *Introduction to WinBUGS for ecologists: A Bayesian approach to regression, ANOVA, mixed models and related analyses*. Academic Press.

Lachish, S., Gopalaswamy, A. M., Knowles, S. C. L., & Sheldon, B. C. (2012). Site-occupancy modelling as a novel framework for assessing test sensitivity and estimating wildlife disease prevalence from imperfect diagnostic tests. *Methods in Ecology and Evolution*, *3*, 339–348. https://doi.org/10.1111/j.2041-210X.2011.00156.x

Muneza, A. B., Ortiz-Calo, W., Packer, C., Cusack, J. J., Jones, T., Palmer, M. S., Swanson, A., Kosmala, M., Dickman, A. J., Macdonald, D. W., & Montgomery, R. A. (2019). Quantifying the severity of giraffe skin disease via photogrammetry analysis of camera trap data. *Journal of Wildlife Diseases*, *55*(4), 770–781. https://doi.org/10.7589/2018-06-149

Murray, M., Cembrowski, A., Latham, A. D. M., Lukasik, V. M., Pruss, S., & St Clair, C. C. (2015). Greater consumption of protein-poor anthropogenic food by urban relative to rural coyotes increases diet breadth and potential for human-wildlife conflict. *Ecography*, *38*(12). https://doi.org/10.1111/ecog.01128

Murray, M., Edwards, M. A., Abercrombie, B., & St. Clair, C. C. (2015). Poor health is associated with use of anthropogenic resources in an urban carnivore. *Proceedings of the Royal Society B: Biological Sciences*, *282*(1806). https://doi.org/10.1098/rspb.2015.0009

Murray, M. H., Fidino, M., Lehrer, E. W., Simonis, J. L., & Magle, S. B. (2021). Data from: A multi-state occupancy model to non-invasively monitor visible signs of wildlife health with camera traps that accounts for image quality. *Dryad Digital Repository*, https://doi.org/10.5061/dryad.x3ffbg7js

Murray, M. H., Hill, J., Whyte, P., & St. Clair, C. C. (2016). Urban compost attracts coyotes, contains toxins, and may promote disease in urban-adapted wildlife. *EcoHealth*, *13*(2). https://doi.org/10.1007/s10393-016-1105-0

Murray, M. H., & St. Clair, C. C. (2017). Predictable features attract urban coyotes to residential yards. *Journal of Wildlife Management*, *81*(4), 593–600. https://doi.org/10.1002/jwmg.21223

National Climatic Data Center (NCDC). (2019). *National oceanic and atmospheric administration national climatic data center*. Retrieved from https://www.ncdc.noaa.gov/cdo-web/datatools/findstation

National Oceanic and Atmospheric Administration. (2019). *National weather service data*. Retrieved from www.weather.gov

Niedringhaus, K. D., Brown, J. D., Sweeley, K. M., & Yabsley, M. J. (2019). A review of sarcoptic mange in North American wildlife. *International Journal for Parasitology: Parasites and Wildlife*, *9*(April), 285–297. https://doi.org/10.1016/j.ijppaw.2019.06.003

O'Connell, A. F., Nichols, J. D., & Karanth, K. U. (Eds.). (2010). *Camera traps in animal ecology: Methods and analyses*. Springer Science & Business Media.

Oleaga, A., Casais, R., Balseiro, A., Espí, A., Llaneza, L., Hartasánchez, A., & Gortázar, C. (2011). New techniques for an old disease: Sarcoptic mange in the Iberian wolf. *Veterinary Parasitology*, *181*(2–4), 255–266. https://doi.org/10.1016/j.vetpar.2011.04.036

Pence, D. B., & Ueckermann, E. (2002). Sarcoptic mange in wildlife. *Revue Scientifique et Technique-Office International Des Epizooties*, *21*(2), 385–398. https://doi.org/10.20506/rst.21.2.1335

Pérez, J. M., Granados, J. E., Sarasa, M., & Serrano, E. (2011). Usefulness of estimated surface area of damaged skin as a proxy of mite load in the monitoring of sarcoptic mange in free-ranging populations of Iberian wild goat, *Capra pyrenaica*. *Veterinary Parasitology*, *176*(2–3), 258–264. https://doi.org/10.1016/j.vetpar.2010.11.002

Pertuz, S., Puig, D., & Garcia, M. A. (2013). Analysis of focus measure operators for shape-from-focus. *Pattern Recognition*, *46*(5), 1415–1432. https://doi.org/10.1016/j.patcog.2012.11.011

Plummer, M. (2003). JAGS: A program for analysis of Bayesian graphical models using Gibbs sampling. In K. Hornik, F. Leisch, & A. Zeileis (Eds.). *Proceedings of the 3rd international workshop on distributed statistical computing* (Vol. 124, pp. 1–10). DSC 2003.

Poessel, S. A., Breck, S. W., & Gese, E. M. (2016). Spatial ecology of coyotes in the Denver metropolitan area: Influence of the urban matrix.

Journal of Mammalogy, *97*(5), 1414–1427. https://doi.org/10.1093/jmammal/gyw090

Prosser, N. S., Gardner, P. C., Smith, J. A., Goon Ee Wern, J., Ambu, L. N., & Goossens, B. (2016). Body condition scoring of Bornean banteng in logged forests. *BMC Zoology*, *1*(1), 1–8. https://doi.org/10.1186/s40850-016-0007-5

R Core Team. (2020). *R: A language and environment for statistical computing*. R Foundation for Statistical Computing.

Reddell, C. D., Abadi, F., Delaney, D. K., Cain, J. W., & Roemer, G. W. (2021). Urbanization's influence on the distribution of mange in a carnivore revealed with multistate occupancy models. *Oecologia*, 1–12. https://doi.org/10.1007/s00442-020-04803-9

Remais, J., Akullian, A., Ding, L., & Seto, E. (2010). Analytical methods for quantifying environmental connectivity for the control and surveillance of infectious disease spread. *Journal of the Royal Society Interface*, *7*(49), 1181–1193. https://doi.org/10.1098/rsif.2009.0523

Royle, J. A., & Dorazio, R. M. (2008). *Hierarchical modeling and inference in ecology: The analysis of data from populations, metapopulations and communities*. Elsevier.

Rudd, J., Clifford, D., Richardson, D., Cypher, B., Westall, T., Kelly, E., & Foley, J. (2019). Hematologic and serum chemistry values of endangered San Joaquin Kit Foxes (*Vulpes macrotis mutica*) with sarcoptic mange. *Journal of Wildlife Diseases*, *55*(2), 410–415. https://doi.org/10.7589/2017-10-270

Saito, M. U., & Sonoda, Y. (2017). Symptomatic raccoon dogs and sarcoptic mange along an urban gradient. *EcoHealth*, *14*(2), 318–328. https://doi.org/10.1007/s10393-017-1233-1

Steenweg, R., Hebblewhite, M., Kays, R., Ahumada, J., Fisher, J. T., Burton, C., Townsend, S. E., Carbone, C., Rowcliffe, J. M., Whittington, J., Brodie, J., Royle, J. A., Switalski, A., Clevenger, A. P., Heim, N., & Rich, L. N. (2017). Scaling-up camera traps: Monitoring the planet's biodiversity with networks of remote sensors. *Frontiers in Ecology and the Environment*, *15*(1), 26–34. https://doi.org/10.1002/fee.1448

Tabak, M. A., Norouzzadeh, M. S., Wolfson, D. W., Sweeney, S. J., Vercauteren, K. C., Snow, N. P., Halseth, J. M., Di Salvo, P. A., Lewis, J. S., White, M. D., Teton, B., Beasley, J. C., Schlichting, P. E., Boughton, R. K., Wight, B., Newkirk, E. S., Ivan, J. S., Odell, E. A., Brook, R. K., … Miller, R. S. (2019). Machine learning to classify animal species in camera trap images: Applications in ecology. *Methods in Ecology and Evolution*, *10*(4), 585–590. https://doi.org/10.1111/2041-210X.13120

Todd, A. W., Gunson, J. R., & Samuel, W. M. (1981). Sarcoptic mange, an important disease of coyotes and wolves of Alberta, Canada. In J. A. Chapman & D. Pursley (Eds.), *Worldwide Furbearer Conference Proceedings*, Frostburg, MD, pp. 706–729.

U.S. Census Bureau. (2018). *Estimates of resident population change and rankings*. July 1, 2017 to July 1, 2018 – United States – Combined statistical area. Retrieved from https://factfinder.census.gov/faces/tableservices/jsf/pages/productview.xhtml?pid=PEP_2014_PEPANNCHG.US41PRandprodType=table

Werner, C. S., & Nunn, C. L. (2020). Effect of urban habitat use on parasitism in mammals: A meta-analysis. *Proceedings of the Royal Society B: Biological Sciences*, *287*(1927), 20200397. https://doi.org/10.1098/rspb.2020.0397

Wright, W. J., Irvine, K. M., & Higgs, M. D. (2019). Identifying occupancy model inadequacies: Can residuals separately assess detection and presence? *Ecology*, *100*(6), e02703. https://doi.org/10.1002/ecy.2703

SUPPORTING INFORMATION

Additional supporting information may be found online in the Supporting Information section.

How to cite this article: Murray MH, Fidino M, Lehrer EW, Simonis JL, Magle SB. A multi-state occupancy model to non-invasively monitor visible signs of wildlife health with camera traps that accounts for image quality. *J Anim Ecol*. 2021;00:1–12. https://doi.org/10.1111/1365-2656.13515